GeoHealth

RESEARCH ARTICLE

10.1029/2023GH000923

Robbie M. Parks and Cascade Tuholske contributed equally to this work.

Key Points:

- Compared heat stress measures using gridded data sets and in situ data from 17 institutions across 42 states in the contiguous US
- Observed variations in heat measures and weather variables align with Köppen-Geiger climate classifications
- Installing more Wet Bulb Globe Temperature-measuring stations in diverse microclimates is key to better heat exposure prevention strategies

Correspondence to:

Y. Ahn,
yjahn@ku.edu

Citation:

Ahn, Y., Tuholske, C., & Parks, R. M. (2024). Comparing approximated heat stress measures across the United States. *GeoHealth*, *8*, e2023GH000923. https://doi.org/10.1029/2023GH000923

Received 8 AUG 2023
Accepted 10 JAN 2024

Author Contribution:

Conceptualization: Cascade Tuholske
Writing – review & editing: Cascade Tuholske

Comparing Approximated Heat Stress Measures Across the United States

Yoonjung Ahn[1,2], Cascade Tuholske[3,4], and Robbie M. Parks[5]

[1]Geography & Atmospheric Science Department, University of Kansas, Lawrence, KS, USA, [2]Institute of Behavioral Science, University of Colorado Boulder, Boulder, CO, USA, [3]Department of Earth Sciences, Montana State University, Bozeman, MT, USA, [4]GeoSpatial Core Facility, Montana State University, Bozeman, MT, USA, [5]Department of Environmental Health Sciences, Mailman School of Public Health, Columbia University, New York, NY, USA

Abstract Climate change is escalating the threat of heat stress to global public health, with the majority of humans today facing increasingly severe and prolonged heat waves. Accurate weather data reflecting the complexity of measuring heat stress is crucial for reducing the impact of extreme heat on health worldwide. Previous studies have employed Heat Index (HI) and Wet Bulb Globe Temperature (WBGT) metrics to understand extreme heat exposure, forming the basis for heat stress guidelines. However, systematic comparisons of meteorological and climate data sets used for these metrics and the related parameters, like air temperature, humidity, wind speed, and solar radiation crucial for human thermoregulation, are lacking. We compared three heat measures (HI_{max}, $WBGT_{Bernard}$, and $WBGT_{Liljegren}$) approximated from gridded weather data sets (ERA5-Land, PRISM, Daymet) with ground-based data, revealing strong agreement from HI and $WBGT_{Bernard}$ (R^2 0.76–0.95, RMSE 1.69–6.64°C). Discrepancies varied by Köppen-Geiger climates (e.g., Adjusted R^2 HI_{max} 0.88–0.95, $WBGT_{Bernard}$ 0.79–0.97, and $WBGT_{Liljegren}$ 0.80–0.96), and metrological input variables (Adjusted R^2 T_{max} 0.86–0.94, T_{min} 0.91–0.94, Wind 0.33, $Solar_{max}$ 0.38, $Solar_{avg}$ 0.38, relative humidity 0.51–0.74). Gridded data sets can offer reliable heat exposure assessment, but further research and local networks are vital to reduce measurement errors to fully enhance our understanding of how heat stress measures link to health outcomes.

Plain Language Summary Extreme heat threatens human health. Rising intensity and duration of heat days expose more to hot environments. To understand how extreme heat affects human health, it is important to use accurate weather information and measures that reflect people's actual experience of the heat. Heat Index (HI) and Wet Bulb Globe Temperature (WBGT) are commonly used heat stress metrics that are widely used to set exposure guidelines and policies. However, there have been limited comparisons between daily heat measures and weather variables. In this study, we compared three heat measures (HI, $WBGT_{Bernard}$, and $WBGT_{Liljegren}$) derived from three widely used gridded weather data sets (ERA5-Land, PRISM, and Daymet) with ground-based weather observations. The heat measures calculated from both the gridded weather data and the station data showed a reasonably strong agreement. However, the differences varied depending on the climate types. Gridded weather data sets can provide a reliable approach to assessing heat exposure and impacts based on meteorological variables to produce heat measures. However, further research and the establishment of local ground station networks are necessary to reduce measurement errors in exposure and improve accuracy. This will help us better understand the relationship between heat measures and their impact on health outcomes.

1. Introduction

Exposure to extreme heat events is a significant burden on human physiological and mental health and livelihoods in many parts of the world (M. L. Bell et al., 2008; Burke et al., 2018; Heo & Bell, 2019; Parks et al., 2020). According to the Centers for Disease Control and Prevention, an average of 685 people died each year between May and September due to underlying and contributing causes of extreme heat from 1999 to 2009. This death toll is the highest compared to fatalities caused by other extreme weather events, such as tornadoes, in the United States (United States Environmental Protection Agency, 2020). Extreme heat also negatively impacts economic output, from lost labor productivity (Zhang & Shindell, 2021) to damage to infrastructure (J. E. Bell et al., 2018; National Centers for Environmental Information, 2017; Underwood et al., 2017). Understanding extreme heat dynamics will be increasingly important to policymakers as extreme heat events increase in frequency and intensity due to climate change (U.S. Global Change Research Program, 2023).

Epidemiological studies typically have applied dry-bulb temperature (T_{db}, e.g., ambient air temperature measured in the shade) as a daily measure of heat exposure (Baldwin et al., 2023; Parks et al., 2023). However, solar radiation, wind speed, pressure, clothing, and metabolic rate also determine heat stress and health impacts (Adams et al., 2022; Bernard & Iheanacho, 2015; Heo et al., 2019). More comprehensive metrics such as Wet Bulb Globe Temperature (WBGT) (Yaglou & Minaed, 1957), which accounts for temperature humidity, solar radiation, and wind speed (Sousa et al., 2022) and Heat Index (HI) (Steadman, 1979), which is a combination of relative humidity (RH) and ambient air temperature, are increasingly used to study heat stress and exposure (Heo & Bell, 2019; Tuholske et al., 2021). These measures better describe factors influencing human thermoregulation and the physiologic impact of heat than air temperature alone.

Moreover, these measures are considered critical information since an increasing number of public health studies and government regulatory bodies use them to measure heat stress. For example, The United States Occupational Safety and Health Administration also developed guidelines for outdoor workers based on HI. National Institute for Occupational Safety and Health guidelines for outdoor workers are based on WBGT and metabolic rate. Moreover, Grundstein and Cooper (2018) also proposed regional WBGT thresholds and guidelines, considering individuals' heat tolerance, which refers to their ability to withstand and adapt to heat stress. However, despite efforts to establish policies and guidelines, heat tolerance varies among individuals and is influenced by various factors such as age, fitness level, acclimatization, hydration status, and overall health (Gardner et al., 2016).

The US National Weather Service (NWS) provides HI information to implement these guidelines according to the weather information. Additionally, in recent years, the NWS began to provide forecast WBGT information which is developed based on the National Digital Forecast Database (National Weather Service Headquarters, 2022a, 2022b). However, only a few weather stations are equipped with a black-globe thermometer, which is critical to accurately gathering WBGT, and it is thus challenging to provide observed WBGT information for most humans worldwide (Rennie et al., 2021; Uejio et al., 2018).

To overcome the limitations of available in situ station data, researchers have developed various gridded weather data and reanalysis products, as well as several methods to calculate heat stress measures with these products (Bernard & Iheanacho, 2015; Brimicombe et al., 2023; Dimiceli et al., 2011; Liljegren et al., 2008; Spangler & Wellenius, 2021; Stull, 2011; Yaglou & Minaed, 1957). Among the various estimation methods for WBGT, the method proposed by Liliegren ($WBGT_{Liljegren}$) has been considered the most robust under outdoor conditions (Bernard & Iheanacho, 2015; Kong & Huber, 2022; Lemke et al., 2019; Patel et al., 2013). HI, calculated with air temperature and RH (Steadman, 1979), is relatively simple to estimate. Therefore, HI is widely applied in epidemiological light winds (Rothfusz, 1990). In other words, HI is limited in utilization for heat exposure guidelines developed based on metabolic rate. Bernard and Iheanacho (2015) suggested a simplified method to estimate WBGT by establishing a quadratic transformation between HI and $WBGT_{Liljegren}$ that also assumes fixed windspeeds (0.5 m/s) and shade.

Although scholars have introduced several approximation methods for heat measures from gridded weather data, daily RH, wind speed, solar radiation, $WBGT_{Bernard}$, $WBGT_{Liljegren}$, and HI approximations have not been quantitatively compared (Spangler et al., 2019). Gridded weather data showed climate-specific performance differences of approximation due to spatial resolutions and algorithms (Kong & Huber, 2022). Further, numerous studies examined and described thermal comfort with Köppen-Geiger's climatic classification, which developed based on seasonal precipitation and temperature patterns (Djamila & Yong, 2016; Mishra & Ramgopal, 2015). While previous literature has provided evidence of the potential impact of different climates on certain biases (Liljegren et al., 2008), there remains a significant knowledge gap regarding the accuracy of these approximations in various climate change settings (Kong & Huber, 2022).

We build upon previous efforts to compare and validate heat metrics across gridded weather and climate data sets with in situ observations (Ahn et al., 2022). Our aim is to use three commonly used gridded weather data sets in epidemiological studies to conduct an intercomparison of multiple metrics HI_{max}, $WBGT_{Bernard}$,$WBGT_{Liljegren}$) and weather variables according to the Köppen-Geiger climate (Beck et al., 2018). To achieve our goal, we will address the following questions: (a) To what extent do gridded climate data sets accurately estimate RH, wind speed, solar radiation, $WBGT_{Bernard}$, $WBGT_{Liljegren}$, and HI. (b) Which climatic zones have the strongest/weakest

Table 1
Overview of the Meteorological Data Sets and User-Derived Variables

	Station data	ERA5	PRISM	Daymet
Meteorological variables used				
Temporal unit	Hourly	Hourly	Daily	Daily
T	O	O		
T_{max}			O	O
T_{min}			O	O
T_{mean}			O	
RH	O			
$Solar_{avg}$		O		O
$Solar_{max}$	O	O		
10 m U wind component		O		
10 m V wind component		O		
Wind speed	O			
T_d		O		
VPD_{min}			O	
Daily level user-derived variables				
Temporal unit	Daily	Daily	Daily	Daily
T_{mean}				O
T_d	O			
RH_{min}		O	O	O
2 m $wind_{min}$	O	O		
HI_{max}	O	O	O	O
Maximum $WBGT_{Bernard}$	O	O	O	O
Maximum $WBGT_{Liljegren}$	O	O	O	O

association with gridded weather data with in situ data in the contiguous United States (CONUS) which has 26 climate categories.

2. Methodology

2.1. In Situ (Station) Weather Data for Observed Heat Measures

We collected hourly air temperature, RH, solar radiation, and wind speed data from April to October 2018 and 2019 from 924 stations operated by 17 institutions (Colorado State University, 2020; Cooperative Agriculture Weather Network, 2020; High Plains Regional Climate Center (HPRCC), 2020; Illinois State, 2019; Kansas Mesonet, 2017; Michigan State University, 2020; Missouri Mesonet, 2020; New Mexico State University, 2020; North Carolina State University, 2020; North Dakota Agriculture Weather Network Center, 2020; South Alabama, 2020; United States Department of Agriculture, 2020; University of Arizona, 2020; University of Florida, 2020; Washington State University, 2020) (Figure A1). Various studies found that the precision of gridded historical weather data differs across various regional climate zones (Ahn et al., 2022; Behnke et al., 2016). Therefore, we stratified analyses of agreement between data sets by Köppen-Geiger climate categories to understand agreement by climate zone. We regrouped Köppen-Geiger climate categories into six categories arid desert (BWh, BWk), arid steppe (BSh, BSk), cold dry (Dsa, Dsb, Dwa, Dwb), cold no dry (Dfa, Dfb, Dfc), temperate (Cfa, Cfb, Csa, Csb), and tropical (Af, Am, Aw). The arid desert climate had 103 stations (11%), arid steppe had 197 (21%) stations, cold dry had 34 stations (4%), cold no dry had 311 stations (34), the temperate climate had 262 stations (28), and tropical climate had 17 stations (2%) (Table A1).

We derived auxiliary climatic variables needed for the estimation of HI and WBGT as described in Table A3. Table 1 describes user-derived variables from the meteorological data sets. Several stations only provided 10-m wind speed and RH. Therefore, we applied a logarithmic wind profile to approximate 2-m wind speed profiles (Fleagle & Businger, 1981). Considering most stations were in agricultural fields, 0.1 m, which indicates low crops and occasional obstacles, was applied as the roughness length (Z_0). We converted dew point temperature (T_d) from RH and air temperature with the R package "weathermetrics" (Brooke Anderson et al., 2013). Finally, we applied statistical quality control (QC), identifying implausible measurements for the station data (Grassmann et al., 2018; Napoly et al., 2018). This process identified hourly WBGT or HI outliers with z-scores within the upper or lower 0.5% of all hourly WBGT or HI data across the study period. If a station missed more than 20% of study months, the stations were considered erroneous and eliminated from the study (Napoly et al., 2018).

2.2. Gridded Weather Data for Estimated Heat Measures

2.2.1. European Centre for Medium-Range Weather Forecasts (ERA5-Land)

ERA5-Land data provides hourly data sets from 1950 to the present with a 9 km spatial resolution (European Centre for Medium-Range Weather Forecasts, 2021). The ECMRWF developed ERA5-Land based on satellite-observational data with advanced forecast modeling to produce a global reanalysis of weather data (ECMWF, 2018). ERA5-Land is an improved spatial version that has finer spatial resolution compared to ERA5 (30 km). This enhancement is achieved by applying the land surface hydrology (HTESSEL) model (version Cy45r1 of the IFS) using high-resolution atmospheric meteorological data from ERA5. We downloaded hourly ERA5-Land data for downward solar radiation, air temperature, dew point temperature, and 10-m U and V wind components via the "cdsapi" package in Python 3.7. We then calculated RH with dewpoint temperature (T_d) and air temperature with the R package "weathermetrics." For wind speed, we first computed a 10-m wind speed from 10-m U and V components (Table A3). Then we converted the wind from 10-m to 2-m with a log wind profile (Table A3), subsequently computing $WBGT_{Bernard}$, $WBGT_{Liljegren}$, and HI hourly level and selected maximum

Table 2
Linear Regression of Weather Station Observations on Gridded Climate Data Sets Overall and >21°C Average Temperatures

		ERA5				PRISM				Daymet			
	Variables (unit)	R^2	Slope	Y-int	RMSE	R^2	Slope	Y-int	RMSE	R^2	Slope	Y-int	RMSE
All	T_{max} (°C)	0.93	0.97	0.81	2.17	0.86	0.89	2.75	3.2	0.94	0.95	1	1.99
	T_{min} (°C)	0.91	0.94	−0.92	2.99	0.92	0.95	1.05	2.24	0.94	0.97	0.67	2.03
	2 m $wind_{min}$ (m/s)	0.33	0.56	0.19	0.93								
	$Solar_{max}$ (W m^2)	0.38	0.09	178.64	5,607.49								
	$Solar_{avg}$ (W m^2)	0.38	0.25	30	1,232.17					0.3	1.14	−11.99	193.6
	RH_{min} (%)	0.74	0.89	4.45	10.03	0.57	0.77	8.62	13.06	0.51	1.07	−6.26	13.7
	HI_{max} (°C)	0.88	0.69	4.81	5.49	0.85	0.77	4.62	3.89	0.95	0.95	0.61	1.99
	Maximum $WBGT_{Bernard}$ (°C)	0.91	0.76	2.67	3.74	0.86	0.79	3.3	3.26	0.95	0.97	0.21	1.68
	Maximum $WBGT_{Liljegren}$ (°C)	0.80	0.8	−0.34	6.64	0.76	0.78	0.77	6.48	0.85	0.96	1.31	2.97
>21	T_{max} (°C)	0.69	0.78	7	1.91	0.48	0.66	10.54	2.27	0.74	0.86	3.94	1.65
	T_{min} (°C)	0.63	0.84	1.82	2.79	0.76	0.8	4.26	1.95	0.75	0.83	3.61	1.95
	2 m $wind_{min}$ (m/s)	0.31	0.45	0.19	0.87								
	$Solar_{max}$ (W m^2)	0.19	0.06	359.24	5,948.75								
	$Solar_{avg}$ (W m^2)	0.33	0.32	−133.01	1,395.57					0.26	1.32	−91.52	197.65
	RH_{min} (%)	0.78	0.84	6.53	9.79	0.64	0.86	5.32	11.25	0.54	1.28	−16.76	13.87
	HI_{max} (°C)	0.28	0.34	17.7	7.35	0.36	0.4	17.23	4.12	0.7	0.83	4.74	1.79
	Maximum $WBGT_{Bernard}$ (°C)	0.26	0.39	12.87	4.27	0.37	0.43	12.72	2.52	0.71	0.84	3.29	1.16
	Maximum $WBGT_{Liljegren}$ (°C)	0.07	0.24	19.26	7.41	0.13	0.41	13.77	6.75	0.22	0.71	8.22	3.48

daily value. Additionally, we calculated daily average T_d, 2-m wind speed, solar radiation ($Solar_{avg}$), daily maximum air temperature, solar radiation ($Solar_{max}$), daily minimum RH (RH_{min}), and air temperature (T_{min}) for individual variables comparison across data sets (Table 2).

2.2.2. Parameter-Elevation Relationships on Independent Slopes Model (PRISM)

The Parameter-elevation Relationships on Independent Slopes Model (PRISM) data set from Oregon State University provides freely available high-resolution (4 km) daily spatial gridded weather data from 1981—to the near present (Daly et al., 2015; Oregon State University, 2022). Several sources (Daly et al., 1997, 2008a, 2015) described the PRISM methodology. But in brief, PRISM is produced with a spatial-weight regression model that utilizes landscape features, such as elevation and aspect, to predict daily meteorological conditions across the CONUS by interpolating data from a dense network of weather stations, thereby generating mean fields. We used daily maximum temperature (T_{max}), minimum temperature (T_{min}), mean dew point temperature (T_d), minimum vapor pressure deficit (VPD_{min}), and maximum vapor pressure deficit (VPD_{max}). PRISM does not provide daily solar radiation and wind speed data. We applied the ERA5-Land data to calculate $WBGT_{Liljegren}$. PRISM data does not include RH. Therefore, we approximated the minimum RH (RH_{min}) to calculate HI_{max} with the equation in Table A3 with the assumption that RH_{min} occurs at T_{max} (Daly et al., 2015).

2.2.3. Daily Surface Weather and Climatological Summaries (Daymet)

Daymet data provides daily weather and climatology variables calculated with ground-based observations—the Global Historical Climatology Network Daily (GHCN-Daily) data set—and statistical modeling techniques to produce 1-km gridded surface data from 1980 over continental North America, Hawaii, and over Puerto Rico from 1950 (Earth NASA, 2022). The data includes daily T_{max}, T_{min}, downward solar radiation, precipitation, snow water, and day length. Daymet provides daily $Solar_{avg}$, which is an average over the daylight period of the day. To estimate maximum HI (HI_{max}), we calculated the daily RH_{min} with an assumption of $T_D = T_{min}$ all day (Spangler et al., 2022) (Table A3). We downloaded Daymet data via the R package "daymetr" (Hufkens et al., 2018). We calculated T_{mean} with the weighted average of minimum and maximum temperatures (Thornton et al., 2020).

Since Daymet does not generate wind speed data, we applied ERA5-Land wind speed data to calculate $WBGT_{Liljegren}$.

2.3. Calculating Heat Stress Measures (Heat Index, $WBGT_{Bernard}$, and $WBGT_{Liljegren}$)

We calculated three commonly used heat stress measures: daily maximum HI (HI_{max}), maximum $WBGT_{Bernard}$, and maximum $WBGT_{Liljegren}$ from April to October 2018 and 2019 (Table 2). HI was calculated with T_{max} and RH_{min} according to the calculations used by the NWS (Rothfusz, 1990; Steadman, 1979). We calculated $WBGT_{Bernard}$ from HI, according to the quadratic relation established by Bernard and Iheanacho (2015). Because $WBGT_{Bernard}$ does not account for radiated heat and assumes a fixed wind speed (0.5 m/s), $WBGT_{Bernard}$ is akin to indoor or shaded WBGT (Bernard & Iheanacho, 2015). Thus, $WBGT_{Bernard}$ and $WBGT_{Liljegren}$ cannot be directly compared against each other. HI_{max} and $WBGT_{Bernard}$ were calculated with T_{max} and RH_{min} from ERA5-Land, PRISM, and Daymet. Daily HI_{max} was calculated with hourly air temperature and RH and selected from hourly in situ data and ERA5-Land. To estimate HI_{max} with hourly ERA5 data, we first estimated HI at each hour for a given day with hourly air temperature and RH and then selected HI_{max} from the hourly HI data.

We also approximated $WBGT_{Liljegren}$ with the R package "HeatStress" (Casanueva et al., 2019). Liljegren's method to calculate WBGT includes air temperature, dew point temperature, wind speed, solar radiation, and surface pressure as input. This study calculated HI and WBGT and selected the maximum hourly value from the in situ data for each day. We applied maximum solar radiation ($Solar_{max}$), T_{max}, minimum dew point temperature, and minimum wind speed to calculate maximum $WBGT_{Liljegren}$ from PRISM, and Daymet (Weatherly & Rosenbaum, 2017).

2.4. Comparison Analysis

We conducted a linear regression of daily T_{max}, T_{min}, RH_{min}, $Solar_{max}$, mean wind speed, HI_{max}, maximum $WBGT_{Bernard}$, and maximum $WBGT_{Liljegren}$. To analyze the direct and linear concordance between PRISM, ERA5- Land, and Daymet estimates and ground-based meteorological observations at the same point in space, the meteorological observations from stations against the coincident, single-pixel PRISM, ERA5-Land, and Daymet grid cell estimates. To evaluate the alignment between the variables and measures in hot conditions, we additionally performed a linear regression analysis for each variable and measure under conditions where the average temperature exceeds 21°C considering the focus on exposure assessment within the framework of heat-related health impacts (Spangler et al., 2019).

For the comparison analysis, we calculated the goodness of fit (adjusted R^2), slope, and intercept of the lines of best fit, as well as mean square errors (RMSE). Higher R^2 values, lower RMAEs, and slopes closer to one and y-intercepts closer to zero were considered more accurate estimations of the observed data. To suggest the best gridded and HI product for each Köppen-Geiger climate, this study conducted the comparison analysis nationally and according to Köppen-Geiger climate groups (Beck et al., 2018).

3. Results

After the statistical QC process, we included information 916 from the initial 924 stations in our analysis (Figure A1 and Table A2).

3.1. Individual Variables Comparison

We found that in situ data and T_{max} showed a strong relationship (adjusted R^2 0.86 < m < 0.94) across the data sets. T_{min} from the estimated data sets also showed a strong relationship with in situ (adjusted R^2 0.91–0.94). Among the data sets, Daymet showed the smallest RMSE from both T_{max} and T_{min} (T_{max} 1.99°C, T_{min} 2.03°C) and the highest R^2 (T_{max} 0.94, T_{min} 0.94). ERA5-Land's wind speed showed a relatively weak correlation (adjusted R^2: 0.33, RMSE 0.93 7%. $Solar_{max}$ from ERA5-Land data showed a low correlation with in situ data adjusted R^2 was 0.38 and RMSE was 5,607.49 W m^2 $Solar_{avg}$ from ERA5-Land also showed a weak relationship with in situ data adjusted R^2 was 0.38 and RMSE was 1,232.17 W m^2. $Solar_{avg}$ from Daymet data showed even weaker, which showed adjusted R^2 0.30 and 193.6 W m^2. ERA5-Land's RH_{min} showed a significant relationship with station data adjusted R^2 was 0.74 and RMSE was 10.03%. PRISM's RH_{min} adjusted R^2 was 0.57, and RMSE was 13.06. Daymet's RH_{min} showed the weakest relationship with the station data, which adjusted R^2 was 0.51 RMSE 13.

Regression analysis between station data and estimated data sets showed a significant relationship for HI_{min}, $WBGT_{Bernard}$, and $WBGT_{Liljegren}$. The adjusted R^2 of ERA5-Land's HI_{max} was 0.80 and RMSE was 6.64°C. PRISM's adjusted R^2 was 0.85, and RMSE was 3.89°C. Daymet showed the strongest correlation with station data (0.95 and RMSE 1.99°C). The relationship between ERA5-Land, PRISM, and Daymet and station data's $WBGT_{Bernard}$ also showed a strong relationship (adjusted R^2: 0.91, RMSE: 3.74°C, adjusted R^2: 0.86, RMSE: 3.26°C, adjusted R^2: 0.95, RMSE: 1.99°C), $WBGT_{Liljegren}$ (adjusted R^2: 0.80, RMSE: 6.64°C, adjusted R^2: 0.76, RMSE: 6.48°C, adjusted R^2: 0.85, RMSE: 2.97°C) respectively (Table 2).

In the category of temperatures exceeding 21°C, T_{max} and T_{min} exhibited varied degrees of correlation across the data sets. For instance, T_{max} showed a moderate to high correlation with ERA5-Land (R^2: 0.7, RMSE: 1.91°C) and Daymet (R^2: 0.74, RMSE: T_{min} correlates strongly with PRISM (R^2: 0.76, RMSE: 1.95°C) and Daymet (R^2: 0.75, RMSE: 1.95°C). $Wind_{min}$, $Solar_{max}$, $Solar_{avg}$, and RH_{min} revealed mixed results with some data sets not providing sufficient data for comparison. For example, ERA5-Land's $Solar_{avg}$ showed an R^2 of 0.38 and a high RMSE of 1,232.17 W m^2, indicating a less strong relationship.

Furthermore, the HI_{max} and WBGT indices, such as Bernard and Liljegren, displayed significant correlations. For instance, HI_{max} with ERA5-Land shows an R^2 of 0.88 and an RMSE of 5.49°C, while PRISM shows an R^2 of 0.85 and an RMSE of 3.89°C. The WBGT Bernard model also presents strong relationships across the data sets, with Daymet showing an R^2 of 0.95 and the lowest RMSE of 1.99°C.

3.2. Comparing Heat Measures According to the Köppen-Geiger Climate Category

Figures 1a–1f illustrate the relationship between in situ data and derived values from the gridded data according to the Köppen-Geiger climate. Figures 1a, 1d, and 1g show the regression results of HI. Adjusted R^2 ranged from 0.46 to 0.95. Similar results were shown with ERA5-Land, PRISM, and Daymet data. From all data sets, tropical climate showed the lowest adjusted R^2. Meanwhile, cold and no dry climate in ERA5-Land (0.90), Arid Desert climate (0.91) in PRISM, and cold dry climate (0.95) in Daymet data showed the highest R^2.

Figures 1b, 1e, and 1h exhibit the regression results of $WBGT_{Bernard}$. The results show that R^2 was from 0.56 to 0.93 with ERA5-Land data, 0.56–0.93 with PRISM data, 0.46–0.91 with Daymet data. From all estimated data, the tropical climate showed the lowest RMSE. The cold and not dry climate in ERA5-Land (0.92), arid desert climate (0.91) in PRISM, cold dry climate (0.95 in both climates) in Daymet data showed the highest R^2.

Figures 1c, 1f, and 1i describe the regression results of $WBGT_{Liljegren}$. ERA5-Land data also showed was 0.34 (ERA 5) in the tropical climate. A week to strong relationship in most climates (0.37–0.87), and cold-dry climates showed the highest R^2 (0.94). PRISM data showed a moderate relationship from all climates. R^2 ranged from 0.37 to 0.87. Cold and dry, and arid desert climates (0.87) showed the strongest relationship. Daymet R^2 showed strong relationships from most of the Köppen-Geiger climates, which ranged from 0.44 to 0.95. Cold-dry climates showed the highest R^2 (0.96). On the other hand, R^2.

RMSE of HI varied from 1.42 to 9.54°C. The arid desert climate exhibited the lowest RMSE in ERA5-Land (2.80°C), while the highest RMSE was observed in the tropical climate (9.54°C). PRISM data revealed that the lowest RMSE (1.27°C) was discovered in the arid tropical climate, while the highest RMSE (2.8°C) was observed in the arid steppe climate. Daymet data also indicated that the tropical climate had the lowest RMSE (1.75°C), whereas the arid desert climate had the highest RMSE (2.41°C). Overall, Daymet showed the smallest variance in RMSE compared to the other data sets (Figures 2a, 2d, and 2g).

The RMSE of $WBGT_{Bernard}$ ranged from 1.19 to 5.35°C. The arid desert climates exhibited the lowest RMSE (2.08°C) in ERA5-Land, while the tropical climate had the highest RMSE (5.35°C) in ERA5-Land data. Similarly, PRISM data showed that arid desert climates had the lowest RMSE of 1.19°C, while tropical climates had the highest RMSE of 3.04°C. However, Daymet data provided somewhat contradictory results compared to ERA5-Land. The lowest RMSE was found in the tropical climate (1.20°C), while the highest was observed in the arid steppe climate (2.02°C) (Figures 2b, 2e, and 2h).

$WBGT_{Liljegren}$ exhibited a range of RMSE from 1.63 to 8.18°C across the data sets. In ERA5-Land data, the lowest RMSE (5.13°C) was observed in cold no dry climate, while the highest RMSE (8.18°C) was found in arid

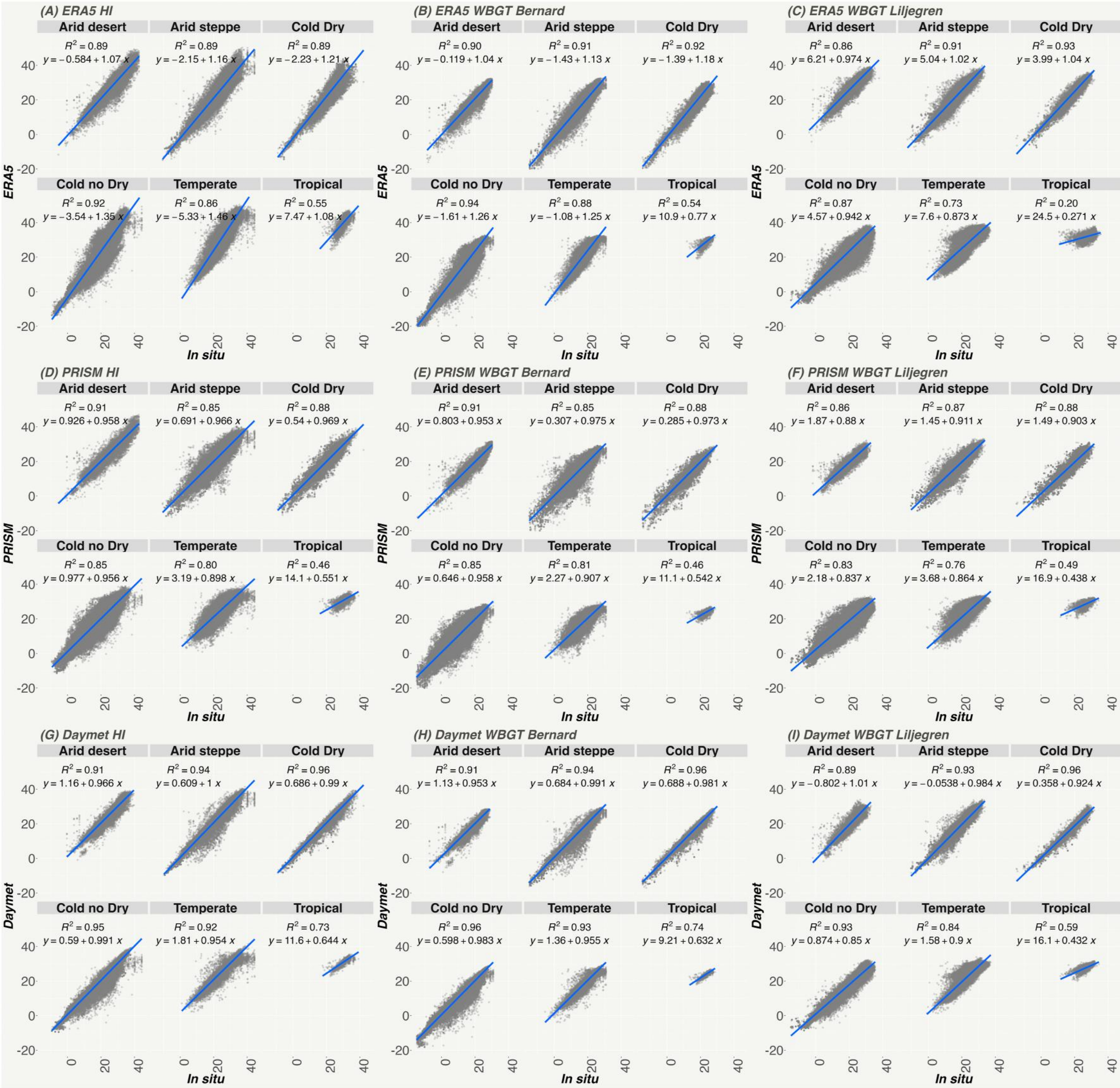

Figure 1. Correlation between heat matrices according to Köppen-Geiger climate.

desert climates. From the PRISM data, the cold no dry climate had the lowest RMSE (4.62°C), and the arid steppe climate had the highest RMSE (6.84°C). Daymet data showed the lowest RMSE (1.63°C) in the cold dry climate and the highest RMSE (2.98°C) in the cold no dry (Figures 2c, 2f, and 2i). Overall, Daymet data demonstrated the smallest variance in RMSE compared to the other data sets. Additionally, most heat indices showed the highest RMSE in the Tropical climate based on ERA5-Land and PRISM data. Daymet data exhibited similar results across the Köppen-Geiger climate (Figures A2 and A3).

4. Discussion

We compared three heat stress measures (HI_{max}, $WBGT_{Bernard}$, and $WBGT_{Liljegren}$) from PRISM, Daymet, and ERA5-Land data with in situ observations for the CONUS. All heat stress measures were highly correlated with observation data (overall temperature R^2 ranged from 0.85 to 0.95) across the three gridded weather data—however, we found that the strength of correlation varied considerably by climate zone in the CONUS and the correlation with ground observations diminish slightly in scenarios where temperatures exceed 21°C across the three gridded weather data.

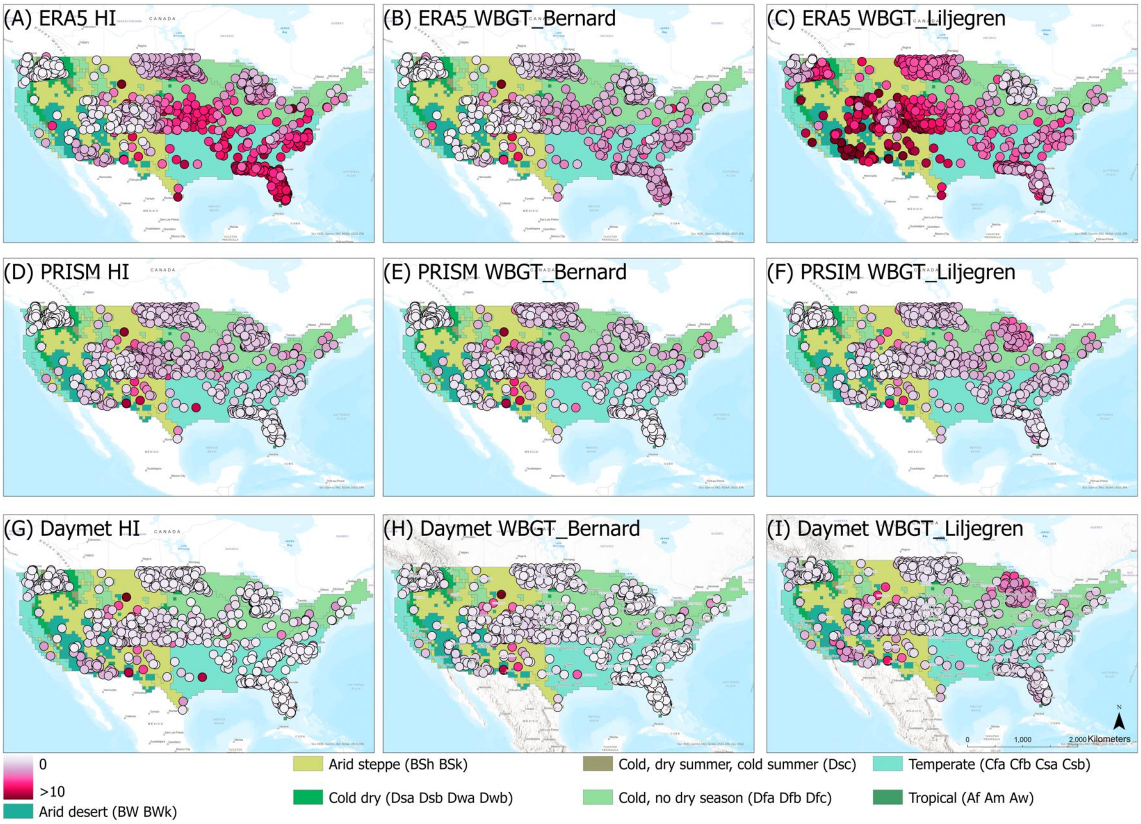

Figure 2. RMSE of heat matrices according to Köppen-Geiger climate.

The correlations (R^2 values) for both T_{max} and T_{min} are generally higher for overall temperatures compared to when temperatures exceed 21°C across all three data sets (ERA5-Land, PRISM, Daymet). For all variables under study, R^2 and RMSE values are generally lower than temperatures of >21°C. Among the gridded data sets, Daymet consistently shows the strongest correlation and the lowest RMSE in both overall and >21°C temperatures, indicating its higher accuracy and reliability in capturing temperature variations compared to ERA5-Land and PRISM. Our analysis indicates that the approach of using T_{max}, RH_{min}, $Solar_{max}$, and $Wind_{min}$ to estimate daily maximum $WBGT_{Liljegren}$ may be less effective at higher temperatures. In other words, relying on these variables could oversimplify the capture of detailed and comprehensive heat stress metrics, potentially reducing accuracy. However, it's noteworthy that the $WBGT_{Bernard}$ and HI measures in the Daymet data set maintained high accuracy for temperatures exceeding 21°C, outperforming other data sets in this regard.

The complex interaction between the input variables used to calculate HI and WBGT may offer an explanation for the observed discrepancies. ERA5-Land and PRISM data showed the lowest RMESs and higher R^2 in tropical climates among the estimated data from all heat measurements. Another possible source of the differences could be the model's algorithms considering cloudiness, sea breeze dynamics, and coastal approximation (Y. Chen et al., 2018; Colle, 2003; Daly et al., 2008b; Perry & Hollis, 2005).

We found estimations of solar radiation were overall poor. According to previous studies, ERA5 solar radiation data showed a better estimation in desert areas due to a higher proportion of days with clear sky conditions in the desert (Andrews et al., 2012; Yang & Bright, 2020). On the other hand, Daymet estimation showed better performance in tropical climates than in other climates. Slater (2016) applied hourly solar radiation data gathered from non-profit organizations in North America and found that Daymet solar radiation tended to have bigger differences in arid deserts, arid steppe, and temperate climates (e.g., California, Florida, Texas, Colorado, New Mexico, and Wyoming State).

Among the gridded weather data, Daymet showed the smallest variance of R^2 and RMSE in different Köppen-Geiger climates. ERA5-*Land* showed higher correlations and smaller RMSE from RH than Daymet. However, Daymet showed a stronger correlation of temperature than PRISM and ERA5-Land, which likely caused higher R^2 and RMSE of HI and WBGT. This finding contradicts previous studies, which have suggested that PRISM performed better than Daymet (Daly et al., 2015; Spangler et al., 2019). A possible explanation might be that the recent update of Daymet data reduced inconsistencies and bias and improved accuracy and precision (Thornton et al., 2021). Additionally, different data processing techniques applied to this study compared to the previous studies might have resulted in different outcomes. Moreover, it is challenging to explain heat measures' relationship with the specific variable analysis outcomes directly since the effect of RH on HI is nonlinear according to Ta increase, and WBGT is the weighted sum of natural wet bulb temperature, black globe temperature, and air temperature (Chakraborty et al., 2022).

Overall RMSE ranged from 1.42 to 9.54°C, 1.19 to 5.35°C, and 1.63 to 9.79°C respectively for HI, $WBGT_{Bernard}$, and $WBGT_{Liljegren}$ across the data sets. The tropical climate, characterized by high air temperature and humidity, which necessitates more complex heat stress measures, exhibited the smallest R^2 and largest RMSE. For instance, ERA5-Land overall showed robust results except for the tropical climate. Since many occupational heat exposure guidelines are formulated according to the HI or WBGT, heat measures are critical information for activity/work and rest decisions (National Institute for Occupational Safety and Health [NIOSH], 2016; The National Oceanic and Atmospheric Administration, 2023). A difference as small as 2–3°C in WBGT and HI can have a significant impact on recommended activity modifications, potentially leading to drastically different health outcomes. This is particularly crucial when strict thresholds are applied in work/rest schedule guidelines. Similarly, a 5–10°C variation in HI can also mislead the application of these guidelines, with similar risks to health. Further work is required to establish fine-scale data that considers local variability caused by complex topography, land use, and building heterogeneity to understand local microclimates further (S. Carter et al., 2018; H. Chen et al., 2010; Klinges et al., 2022; Oke, 1982; Tripp et al., 2020). Some studies suggested a fine spatial scale (10–25 m) is necessary to capture mountain terrain and ocean effects (Dadic et al., 2010; Du Vivier & Cassano, 2013; Gultepe, 2015; Liston, 2004; Mott et al., 2008).

Of the individual weather variables (T_{max}, T_{min}, RH_{min}, wind speed, and solar radiation), T_{max} and T_{min} showed the highest R^2 and lowest RMSE. Wind speed, solar radiation, and RH showed relatively lower R^2 and higher RMSE. Lower correlations of solar radiation, wind speed, and RH between gridded weather data and station data are consistent with other research which compared station data with gridded weather data (Bonshoms et al., 2022; A. W. Carter et al., 2020; Jared Rennie et al., 2021; Rupp et al., 2022; Slater, 2016; Spangler et al., 2022).

Spangler et al. (2019) compared Daymet data with US Climate Reference Network (USCRN) data and showed that RH_{min} showed a relatively low R^2 (0.52). Another study that compared Automated Surface Observing Systems and USCRAN data showed lower correlation coefficients in wind speed (coefficient 0.4) (Rennie et al., 2021). The mean of the absolute error was eight percent different from the comparison analysis with hourly solar radiation data from the National Renewable Energy Laboratory database and several gridded weather data sets, including Daymet and PRISM (Rupp et al., 2022). Bonshoms et al. (2022) validated ERA5-Land RH data with Automatic Weather Stations data from eight stations in four study areas on a glacier and discovered that the R^2 ranged from 0.3 to 0.6.

The discrepancies between station data and gridded weather data have been discussed in the broader literature. Comparison of the findings with those of other studies confirms that one of the major causes was geographical features such as elevation, topography, proximation to coastlines, cloud cover, and land use (Barry, 2008; Daly et al., 2008b; Du Vivier & Cassano, 2013; Gultepe, 2015; Gultepe et al., 2014; Karger et al., 2021; Kilpelainen et al., 2011; Monson & Baldocchi, 2014; Reeve & Kolstad, 2011; Thornton et al., 1997). Previous studies found complex terrain creates local climates that alter solar radiation reflection and wind flows (Hilliker et al., 2010; Slater, 2016; Yang & Bright, 2020; Zardi & Whiteman, 2013). Tscholl et al. (2022) applied cloud cover correction and included solar radiation to estimate 100m spatial resolution air temperature, and the cloud correction model reduced the mean absolute error of estimated air temperature by 23% compared with the clear-sky model.

Moreover, land use and land cover were suggested as other factors causing the differences. Land use and land cover create different interactions between the biosphere and atmosphere via heat, water, and energy fluxes. Due to these phenomena, adjacent land can have different local climates, and it has been challenging to consider in the model (Albergel et al., 2018; Page et al., 2018; Zardi & Whiteman, 2013). Chakraborty et al. (2022) examined urban-rural differences in HI and found that urban form alters RH and heat stress in Europe. Vegetation cover in urban areas is often recommended to reduce air temperature and heat exposure. However, vegetation cover does not necessarily correspond to a decrease in air temperature, and vegetation evaporation would increase RH, leading to an increase in HI (Chakraborty et al., 2022). Additionally, the differences might be caused by user-derived variables such as RH, T_{mean}, and T_d. This study derived RH with air, dew point temperatures, and vapor-pressure deficits from the three gridded weather data sets this study applied in this study. For example, this study assumed that T_d is equal to T_{min} throughout the day to calculate RH_{min} from PRISM, and RH_{min} occurs at T_{max} from Daymet to calculate RH_{min} (Thornton et al., 1997).

Our study does have limitations. First is the geographic distribution of weather stations. Only 17 stations (2%) are in the tropical climate, and no stations were from cold, dry summer and cold summer climates. Moreover, higher discrepancies in tropical climate might be caused by the methodology used to calculate daily maximum heat measures. While observation and ERA5-Land RH_{min}, T_{min}, and T_{max} from Daymet and PRISM. Consequently, we advise readers to interpret these results with caution. Further investigation should be conducted to consider various climates more accurately. This study also applied wind speed and solar radiation data from ERA5-Land for estimating heat measures from PRISM and Daymet. We acknowledge that employing data with varying spatial resolutions could lead to certain implications in our results.

Additionally, we approximated several variables and heat measures with several assumptions. Installing additional stations that directly measure WBGT at diverse microclimates (rural, suburban, and urban regions) to enhance field data collection in diverse microclimates will be essential to preventive measures against heat exposure. This will also enable us to investigate further the relationship between estimating heat measures across microclimates within different climate zones. More specifically, in our calculations of the HI_{max}, we used the RH_{min} and T_{max}. This approach assumes that RH tends to decrease as temperature increases. It's important to note that the validity of the HI calculation is applicable primarily in shaded conditions.

Finally, it is important to note that at any location, T_a, RH, radiation, and wind speed might not align in their diurnal patterns, potentially impacting our estimates of HI_{max} and WBGT. For instance, Justine et al. (2023) observed that the peak wet bulb temperature often occurs several hours after the peak dry bulb temperature. In tropical areas near coasts or rivers, where temperature (T) variation throughout the day is minimal, the afternoon influence of the water body can result in higher daily HI or $WBGT_{max}$ compared to when the T_{max} happens. The complexity of these factors underscores the need for more research to accurately assess how the diurnal cycle influences the peak hour of heat stress (Justine et al., 2023; Rusticucci & Vargas, 1995). Given the complexity of the inputs, assessing the impacts of the diurnal cycle on estimating the hour of maximum heat stress will require further research.

5. Conclusion

We examined three heat measures with Daymet, PRISM, and ERA5-Land. The heat measures, which were calculated from Daymet, PRISM, and ERA5-Land and station data, showed strong relationships (R^2 0.82–0.96, RMSE 1.69–5.37°C). However, the discrepancies varied according to Köppen-Geiger climates and warmer conditions (average temperature >21°C). We need to conduct further work to gather more accurate and higher-resolution weather information over space and time, which will help reduce bias and uncertainties. We suggested installing more stations to gather WBGT information and develop gridded weather data, including solar radiation and wind speed. Ultimately, this will lead to a more robust understanding between the links between humid heat and health outcomes.

Appendix A

Figure A1 describes the location of stations and grouped Köppen-Geiger climate categories used for this study. Each color on the map corresponds to a different Köppen-Geiger climate classification, while the gray dots indicate the locations of stations where we collected observational data.

Figure A2 illustrates the correlation between the observed data and the data products (ERA5, Daymet, and PRISM) for the variables utilized in this study, categorized according to the Köppen-Geiger climate classification.

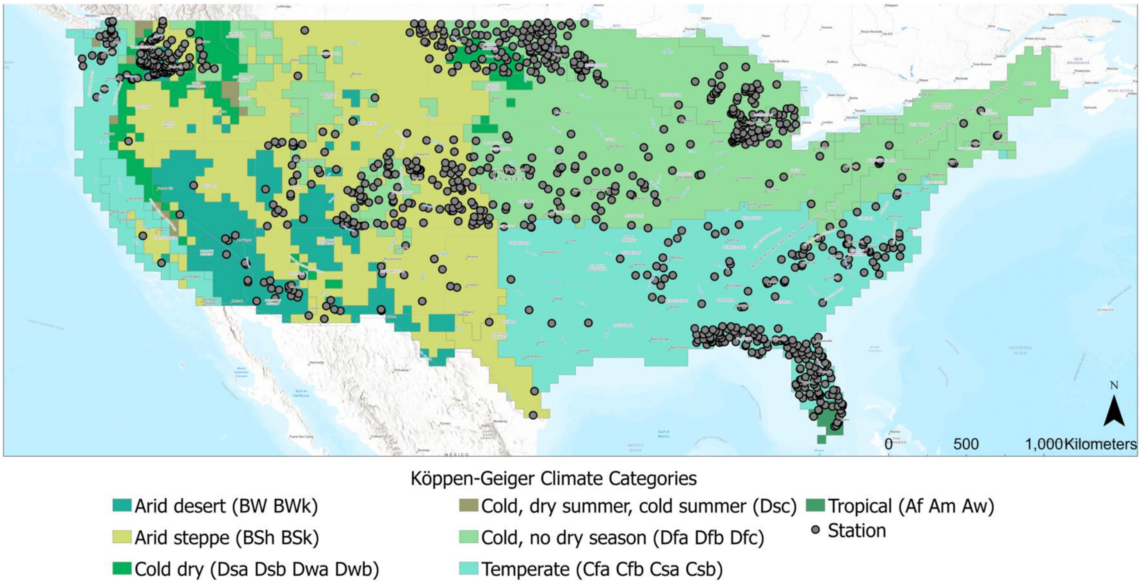

Figure A1. Köppen-Geiger and station locations.

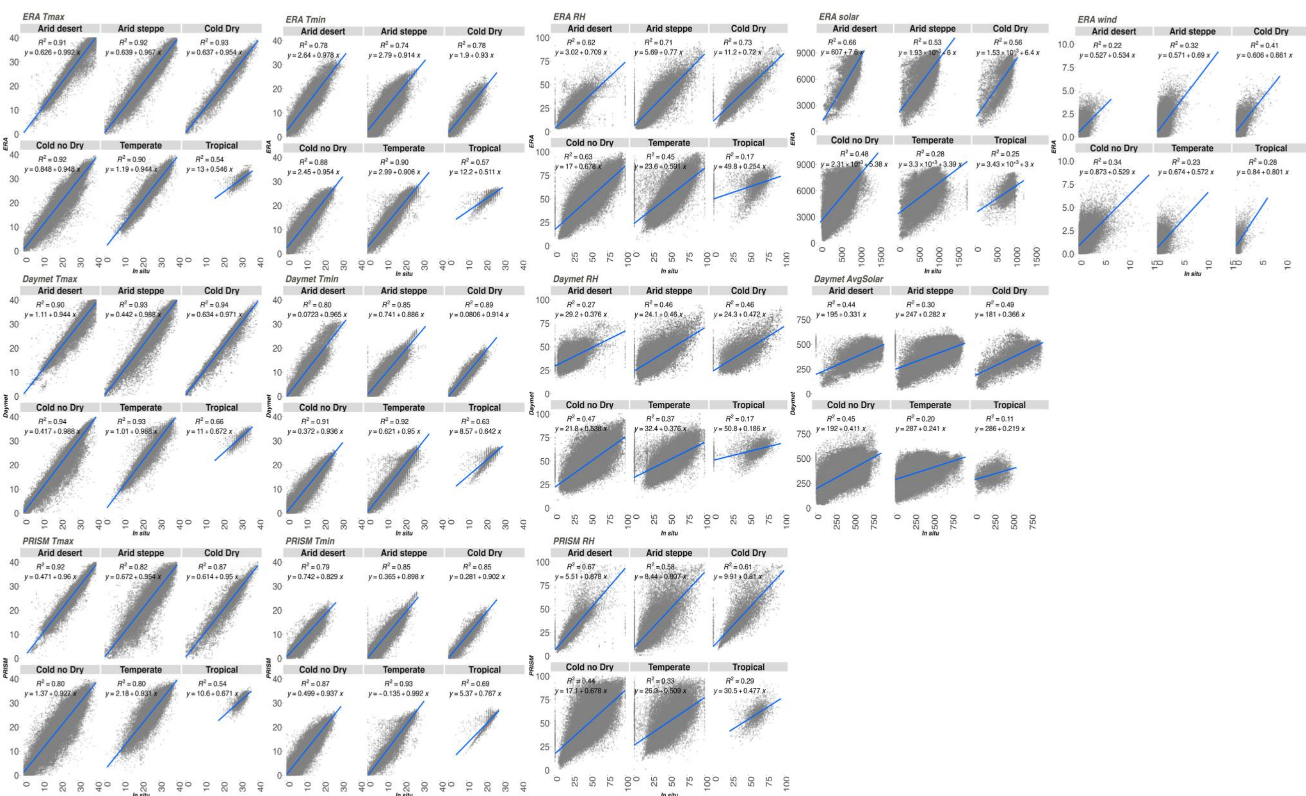

Figure A2. Linear regression of weather station observations on gridded climate data sets according to Köppen-Geiger climates categories.

Table A1 represents the number of stations according to Köppen-Geiger climate categories.

Table A2 shows the number of stations included during the study period (April to October 2018–2019) after the quality control process.

Table A1
Number of Stations According to Köppen-Geiger Climate Categories

Köppen-Geiger climate groups	Köppen-Geiger climate categories	Number of stations (%)	Köppen-Geiger climate groups summary
Arid desert	BWh	20 (2)	103 (11)
Arid desert	BWk	83 (9)	
Arid steppe	BSh	3 (0)	197 (21)
Arid steppe	BSk	194 (21)	
Cold dry	Dsa	1 (0)	34 (4)
Cold dry	Dsb	14 (2)	
Cold dry	Dwa	4 (0)	
Cold dry	Dwb	15 (2)	
Cold no dry	Dfa	157 (17)	311 (34)
Cold no dry	Dfb	145 (16)	
Cold no dry	Dfc	9 (1)	
Temperate	Cfa	233 (25)	262 (28)
Temperate	Cfb	6 (1)	
Temperate	Csa	1 (0)	
Temperate	Csb	22 (2)	
Tropical	Af	4 (0)	17 (2)
Tropical	Am	8 (1)	
Tropical	Aw	5 (1)	

Table A2
Number of Stations Included for the Analysis After Quality

Year	Month	Number of stations
2018	4	696
2018	5	712
2018	6	559
2018	7	559
2018	8	558
2018	9	562
2018	10	479
2019	4	761
2019	5	554
2019	6	558
2019	7	561
2019	8	547
2019	9	524
2019	10	459

Table A3 details the formulas employed for estimating heat stress metrics. The $WBGT_{Liljegren}$ calculation was performed using the "HeatStress" package in R which was developed based on Liljegren et al. (2008) study. The package includes the "esat" function which computes vapor pressure using air temperature and relative humidity, applying the coefficient recommended by (Sonntag, 1990). Additionally, the package includes an algorithm for estimating solar irradiation, taking into account solar radiation, the Earth-Sun distance, and the zenith angle. This algorithm was developed by analyzing a full year of direct and diffuse solar irradiance data, gathered by the Atmospheric Radiation Measurement Program at their facility in north-central Oklahoma (Ackerman &

Table A3
Equations for User-Derived Meteorological Variables

Variable	Data set	Expression	Unit	Note
T_d	In situ	$T_d = T - \left(\frac{100-\mathrm{RH}}{5}\right)$ • T_d = Dew point temperature • T = air temperature • RH = relative humidity	T, T_d in °C RH in %	
2 m wind speed	ERA5, in situ	$V \approx V_{\mathrm{ref}} * \ln \frac{Z* Z_0}{Z_{\mathrm{ref}} * Z_0}$ • V = velocity to be calculated at height z • Z = height above ground level for velocity v • V_{ref} = known velocity at height z_{ref} • Z_{ref} = reference height where v_{ref} is known • Z_0 = roughness length in the current wind direction	m/s	
Hourly solar radiation ($W\ m^2$)	ERA5	$\frac{\text{Hourly solar radiation}}{3600\ [\mathrm{s}]}$	Hourly solar. Radiation in J m^2, s represents second	
RH_{min} (%)	ERA	$100 \cdot \frac{e^{\left(\frac{17.625 \cdot T_D}{243.04°C + T_D}\right)}}{e^{\left(\frac{17.625 \cdot T}{243.04°C + T}\right)}}$ • T_d = Dew point temperature • T = air temperature	T, T_d in °C	Minimum based on hourly values
	PRISM	$100 \cdot \frac{\left[610.94\ \mathrm{Pa} \cdot e^{\left(\frac{17.625 \cdot T_{\max}}{243.04°C + T_{\max}}\right)}\right] - \mathrm{VPD}_{\max}}{610.94\ \mathrm{Pa} \cdot e^{\left(\frac{17.625 \cdot T_{\max}}{243.04°C + T_{\max}}\right)}}$ • $\mathrm{VPD}_{\max}$ = maximum vapor-pressure deficits (VPD)	$T_{\max}$ in °C $\mathrm{VPD}_{\max}$ in Pa	Assumes RH_{min} occurs at $T_{\max}$
	Daymet	$100 \cdot \frac{e^{\left(\frac{17.269 \cdot T_{\min}}{237.3°C + T_{\min}}\right)}}{e^{\left(\frac{17.269 \cdot T_{\max}}{237.3°C + T_{\max}}\right)}}$	$T_{\min}$, $T_{\max}$ in °C	Assumes $T_D = T_{\min}$ all day
T_{mean}	PRISM	$0.606 \cdot T_{\max} + 0.394 \cdot T_{\min}$	$T_{\max}$ in °C	
$HI_{\max}$	ERA5, PRISM, Daymet, in situ	0.5 * {Ta + 61.0 + [(Ta − 68.0)*1.2] + (RH *0.094)} If this heat index value is 80°F or higher, the full equation with adjustments should be applied. −42.379 + 2.04901523* Ta + 10.14333127* RH − 0.22475541*Ta* RH − 0.00683783* Ta^2 − 0.05481717*RH^2 + 0.00122874*Ta^2* RH + 0.00085282* Ta *RH^2 − 0.00000199*Ta^2 *RH^2 − ADJ *Condition 1: RH < 13% and T_a is between 80 and 112°F • $\mathrm{ADJ}_1 = -[(13 - \mathrm{RH})/4] * \sqrt{((17 - T_a - 95)/17)}$	T_a in °FRH in %, $T_{\max}$ and RH_{min} were applied instead for Ta and RH for ERA5, PRISM, and Daymet	

Table A3
Continued

Variable	Data set	Expression	Unit	Note
		* Condition 2: RH > 85% and T_a is between 80 and 87°F $\mathrm{ADJ}_2 = ((\mathrm{RH} - 85)/10)*((87 - T_a)/5)$ T_a = Ambient Dry Bulb Temperature • RH = relative humidity		
$\mathrm{WBGT}_{\mathrm{Bernard}}$	ERA5, PRISM, Daymet, in situ	$-0.0034*\mathrm{HI}*2 + 0.96*\mathrm{HI} - 34$ • HI = Heat Index	HI in °F	
$\mathrm{WBGT}_{\mathrm{Liljegren}}$	ERA5, PRISM, Daymet, in situ	$0.7*\mathrm{Tw} + 0.2*\mathrm{Tg} + 0.1*\mathrm{Ta}$ • T_w: Wet-Bulb Temperature • T_g: Globe Temperature • T_a: Dry Bulb Temperature $\mathrm{WS} = \sqrt{(uwd^2 + vwd^2)}$ • WS: wind speed • *uwd*: 10 m U wind component • *vwd*: 10 m V wind component $\text{Vapor pressure} = a*\exp\left(\frac{\left(\frac{b*T_{\mathrm{air}}}{c+T_{\mathrm{air}}}\right)}{100}\right)$ $a = 611.2$, $b = 17.62$, and $c = 243.12$ $F_{\mathrm{dir}} = \begin{cases} \exp\left(3 - 1.34S^* - \frac{1.65}{S^*}\right) & \theta \le 89.5^\circ \\ 0, \theta > 89.5^\circ \end{cases}$ F_{dir} = solar irradiation $S^* = \frac{S}{S_{\max}}$ $S_{\max} = \frac{S_0 \cos\theta}{d^2}\ (\theta \le 89.5^\circ)$ S_0 = solar constant (=1,367 W/m^2) θ = Zenithangle and d = earth-sun direction		

Stokes, 2003). For accurate $\mathrm{WBGT}_{\mathrm{Liljegren}}$ calculations using the HeatStress package, users must input variables such as time, latitude, and longitude to determine the zenith angle.

Figure A4 illustrates the daily maximum temperature from Daymet, PRISM, and air temperature at 2 p.m. ERA5-Land on 1 August 2018, alongside the locations of the stations from which we collected observational data.

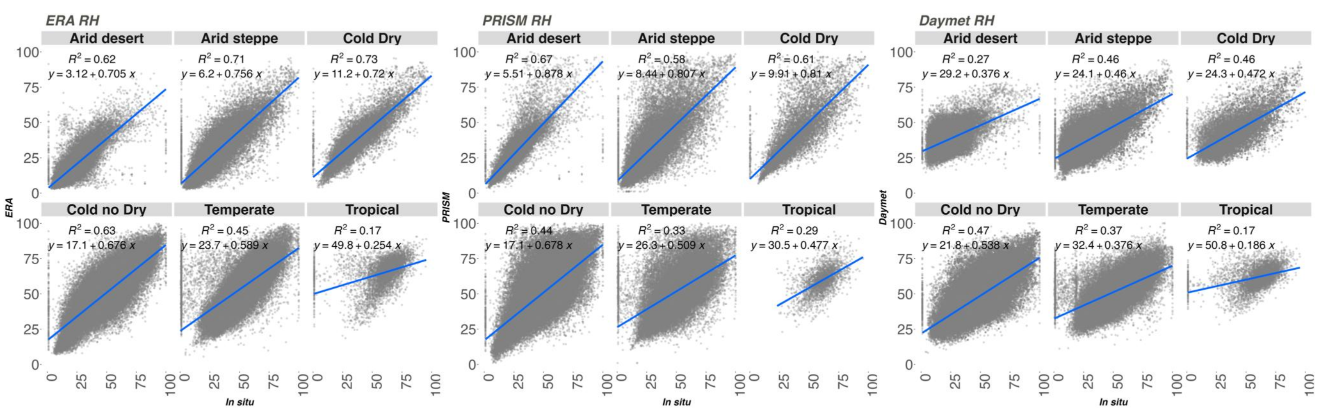

Figure A3. Linear regression of weather station observations on gridded climate data sets according to Köppen-Geiger climates categories (relative humidity without zeros).

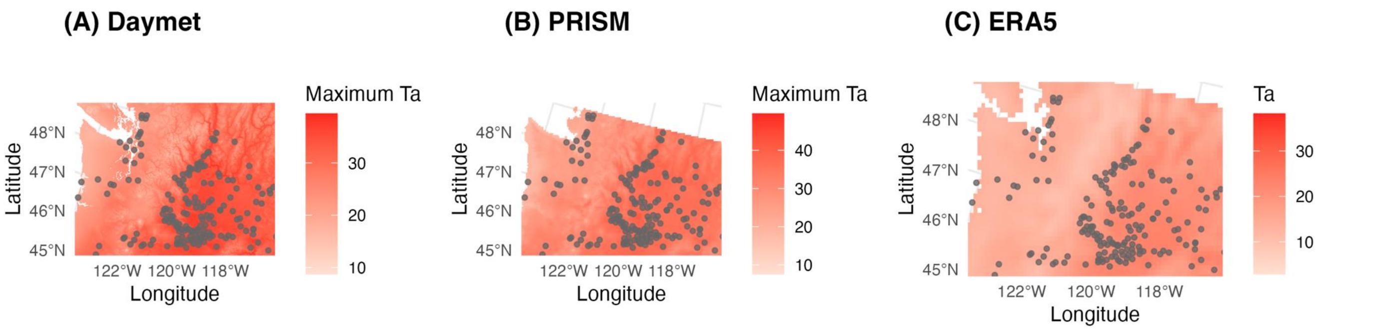

Figure A4. Gridded weather data and station locations across Washington areas (Daymet and PRISM data sets represent daily maximum temperatures, while the ERA5 data set illustrates the air temperature at 2 p.m. on 1 August 2018).

Conflict of Interest

The authors declare no conflicts of interest relevant to this study.

Data Availability Statement

ERA5-Land (European Centre for Medium-Range Weather Forecasts, 2021), PRISM (Oregon State University, 2022), Daymet (Earth NASA, 2022), were used for calculating estimated WBGT. The in station WBGT was calculated from the data sets that were gathered from 17 institutes (Colorado State University, 2020; Cooperative Agriculture Weather Network, 2020; Illinois State, 2019; Kansas Mesonet, 2017; Michigan State University, 2020; Missouri Mesonet, 2020; North Carolina State University, 2020; North Dakota Agriculture Weather Network Center, 2020; South Alabama, 2020; STEM, 2020; University of Arizona, 2020; University of Florida, 2020). The quality control method (Napoly et al., 2018) was applied for the in station WBGT data. Köppen-Geiger climate classification at a 1-km resolution for a contemporary climatology period (1980–2016) from Beck et al. (2018). Figures were made with the package "ggplot2" in R (version 4.1.0). The code for calculating HI (Tuholske, 2021) and downloading ERA5 (Parks, 2022) is available on GitHub. The storage of the data set is licensed under Harvard Dataverse (Ahn, 2022).

Acknowledgments
Dr. Ahn would like to express sincere gratitude to the Department of Geography and Atmospheric Science Department at the University of Kansas for the grant and support. Additionally, her appreciation extends to the two anonymous reviewers whose insightful comments significantly contributed to the enhancement of this research.

References

Ackerman, T. P., & Stokes, G. M. (2003). The atmospheric radiation measurement program. *Physics Today*, *56*(1), 38–44. https://doi.org/10.1063/1.1554135

Adams, Q. H., Sun, Y., Sun, S., & Wellenius, G. A. (2022). Internet searches and heat-related emergency department visits in the United States. *Scientific Reports*, *12*(1), 9031. https://doi.org/10.1038/s41598-022-13168-3

Ahn, Y. (2022). Verifying experimental wet bulb globe temperature hindcasts across the United States [Dataset]. Harvard Dataverse. https://doi.org/10.7910/DVN/2HMGVH

Ahn, Y., Uejio, C. K., Rennie, J., & Schmit, L. (2022). Verifying experimental wet bulb globe temperature hindcasts across the United States. *GeoHealth*, *6*(4), e2021GH000527. https://doi.org/10.1029/2021gh000527

Albergel, C., Munier, S., Bocher, A., Bonan, B., Zheng, Y., Draper, C., et al. (2018). LDAS-Monde sequential assimilation of satellite derived observations applied to the contiguous US: An ERA-5 driven reanalysis of the land surface variables. *Remote Sensing*, *10*(10), 1–24. https://doi.org/10.3390/rs10101627

Andrews, G. J., Evans, J., Dunn, J. R., & Masuda, J. R. (2012). Arguments in health Geography: On sub-disciplinary progress, observation, translation. *Geography Compass*, *6*(6), 351–383. https://doi.org/10.1111/j.1749-8198.2012.00490.x

Baldwin, J. W., Benmarhnia, T., Ebi, K. L., Jay, O., Lutsko, N. J., & Vanos, J. K. (2023). Humidity's role in heat-related health outcomes: A heated debate. *Environmental Health Perspectives*, *131*(5). https://doi.org/10.1289/EHP11807

Barry, R. G. (2008). Mountain weather and climate. In *Mountain weather and climate* (3rd ed., pp. 1–506). https://doi.org/10.1017/CBO9780511754753

Beck, H. E., Zimmermann, N. E., McVicar, T. R., Vergopolan, N., Berg, A., & Wood, E. F. (2018). Present and future Köppen-Geiger climate classification maps at 1-km resolution. *Scientific Data*, *5*(1), 180214. https://doi.org/10.1038/sdata.2018.214

Behnke, R., Vavrus, S., Allstadt, A., Albright, T., Thogmartin, W. E., & Radeloff, V. C. (2016). Evaluation of downscaled, gridded climate data for the conterminous United States. *Ecological Applications*, *26*(5), 1338–1351. https://doi.org/10.1002/15-1061

Bell, J. E., Brown, C. L., Conlon, K., Herring, S., Kunkel, K. E., Lawrimore, J., et al. (2018). Changes in extreme events and the potential impacts on human health. *Journal of the Air and Waste Management Association*, *68*(4), 265–287. https://doi.org/10.1080/10962247.2017.1401017

Bell, M. L., O'Neill, M. S., Ranjit, N., Borja-Aburto, V. H., Cifuentes, L. A., & Gouveia, N. C. (2008). Vulnerability to heat-related mortality in Latin America: A case-crossover study in São Paulo, Brazil, Santiago, Chile and Mexico City, Mexico. *International Journal of Epidemiology*, *37*(4), 796–804. https://doi.org/10.1093/ije/dyn094

Bernard, T. E., & Iheanacho, I. (2015). Heat index and adjusted temperature as surrogates for wet bulb globe temperature to screen for occupational heat stress. *Journal of Occupational and Environmental Hygiene*, *12*(5), 323–333. https://doi.org/10.1080/15459624.2014.989365

Bonshoms, M., Ubeda, J., Liguori, G., Körner, P., Navarro, Á., & Cruz, R. (2022). Validation of ERA5-Land temperature and relative humidity on four Peruvian glaciers using on-glacier observations. *Journal of Mountain Science*, *19*(7), 1849–1873. https://doi.org/10.1007/s11629-022-7388-4

Brimicombe, C., Lo, C. H. B., Pappenberger, F., Di Napoli, C., Maciel, P., Quintino, T., et al. (2023). Wet bulb globe temperature: Indicating extreme heat risk on a global grid. *GeoHealth*, *7*(2), e2022GH000701. https://doi.org/10.1029/2022GH000701

Brooke Anderson, G., Bell, M. L., & Peng, R. D. (2013). Methods to calculate the heat index as an exposure metric in environmental health research. *Environmental Health Perspectives*, *121*(10), 1111–1119. https://doi.org/10.1289/EHP.1206273

Burke, M., González, F., Baylis, P., Heft-Neal, S., Baysan, C., Basu, S., & Hsiang, S. (2018). Higher temperatures increase suicide rates in the United States and Mexico. *Nature Climate Change*, *8*(8), 723–729. https://doi.org/10.1038/s41558-018-0222-x

Carter, A. W., Zaitchik, B. F., Gohlke, J. M., Wang, S., & Richardson, M. B. (2020). Methods for estimating wet bulb globe temperature from remote and low-cost data: A comparative study in central Alabama. *GeoHealth*, *4*(5), e2019GH000231. https://doi.org/10.1029/2019GH000231

Carter, S., Green, J., & Speed, E. (2018). Digital technologies and the biomedicalisation of everyday activities: The case of walking and cycling. *Sociology Compass*, *12*(4), 1–12. https://doi.org/10.1111/soc4.12572

Casanueva, A., Kotlarski, S., Herrera, S., Fischer, A. M., Kjellstrom, T., & Schwierz, C. (2019). Climate projections of a multivariate heat stress index: The role of downscaling and bias correction. *Geoscientific Model Development*, *12*(8), 3419–3438. https://doi.org/10.5194/gmd-12-3419-2019

Chakraborty, T., Venter, Z. S., Qian, Y., & Lee, X. (2022). Lower urban humidity moderates outdoor heat stress. *AGU Advances*, *3*(5), e2022AV000729. https://doi.org/10.1029/2022AV000729

Chen, H., Zeng, D., & Yan, P. (2010). *Public health syndromic surveillance systems* (pp. 9–31). Springer. https://doi.org/10.1007/978-1-4419-1278-7_2

Chen, Y., Shen, H., Smith, K. R., Guan, D., Chen, Y., Shen, G., et al. (2018). Estimating household air pollution exposures and health impacts from space heating in rural China. *Environment International*, *119*, 117–124. https://doi.org/10.1016/j.envint.2018.04.054

Colle, B. A. (2003). An investigation of terrain-atmosphere-ocean interactions along the coastal regions of North America. Retrieved from http://www.onr.navy.mil/sci_tech/ocean/onrpgabr.htm

Colorado State University. (2020). Colorado's Mesonet (CoAgMET) [Dataset]. Retrieved from https://coagmet.colostate.edu/

Cooperative Agriculture Weather Network. (2020). Columbia-pacific northwest region programs [Dataset]. Retrieved from https://www.usbr.gov/pn/agrimet/agrimetmap/agrimap.html

Dadic, R., Mott, R., Lehning, M., & Burlando, P. (2010). Wind influence on snow depth distribution and accumulation over glaciers. *Journal of Geophysical Research*, *115*(F1), F01012. https://doi.org/10.1029/2009JF001261

Daly, C., Halbleib, M., Smith, J. I., Gibson, W. P., Doggett, M. K., Taylor, G. H., et al. (2008a). Physiographically sensitive mapping of climatological temperature and precipitation across the conterminous United States. *International Journal of Climatology*, *28*(15), 2031–2064. https://doi.org/10.1002/joc.1688

Daly, C., Halbleib, M., Smith, J. I., Gibson, W. P., Doggett, M. K., Taylor, G. H., & Pasteris, P. P. (2008b). The impact of the positive Indian Ocean dipole on Zimbabwe droughts Tropical climate is understood to be dominated by. *International Journal of Climatology*, *2029*, 2011–2029. https://doi.org/10.1002/joc

Daly, C., Smith, J. I., & Olson, K. V. (2015). Mapping atmospheric moisture climatologies across the conterminous United States. *PLoS One*, *10*(10), e0141140. https://doi.org/10.1371/journal.pone.0141140

Daly, C., Taylor, G., & Gibson, W. (1997). The prism approach to mapping precipitation and temperature.

Dimiceli, V. E., Piltz, S. F., & Amburn, S. A. (2011). *World congress on engineering and computer science: WCECS 2011: 19-21 October, 2011*. Newswood Ltd., International Association of Engineers.

Djamila, H., & Yong, T. L. (2016). A study of Köppen-Geiger system for comfort temperature prediction in Melbourne city. *Sustainable Cities and Society*, *27*, 42–48. https://doi.org/10.1016/j.scs.2016.08.009

Du Vivier, A. K., & Cassano, J. J. (2013). Evaluation of WRF model resolution on simulated mesoscale winds and surface fluxes near Greenland. *Monthly Weather Review*, *141*(3), 941–963. https://doi.org/10.1175/MWR-D-12-00091.1

Earth NASA. (2022). Daymet [Dataset]. Retrieved from https://daymet.ornl.gov/

ECMWF. (2018). IFS documentation CY45R1 - Part IV: Physical processes | ECMWF [Dataset]. Retrieved from https://www.ecmwf.int/en/elibrary/80895-ifs-documentation-cy45r1-part-iv-physical-processes

European Centre for Medium-Range Weather Forecasts. (2021). ERA5 | ECMWF. Retrieved from https://www.ecmwf.int/en/forecasts/datasets/reanalysis-datasets/era5

Fleagle, R. G., & Businger, J. A. (1981). An introduction to atmospheric physics (Academic Press, Ed.). Retrieved from https://books.google.com/books?hl=en&lr=&id=qgWHwX0IpdAC&oi=fnd&pg=PP1&dq=An+introduction+to+Atmospheric+Physics&ots=XuLHlq7zFF&sig=xDh45_WO8pE3BdflVgHeH-YjGuw#v=onepage&q=An%20introduction%20to%20Atmospheric%20Physics&f=false

Gardner, J. L., Amano, T., Sutherland, W. J., Clayton, M., & Peters, A. (2016). Individual and demographic consequences of reduced body condition following repeated exposure to high temperatures. *Ecology*, *97*(3), 786–795. https://doi.org/10.1890/15-0642.1

Grassmann, T., Napoly, A., Meier, F., & Fenner, D. (2018). DepositOnce: Quality control for crowdsourced data from CWS. Retrieved from https://depositonce.tu-berlin.de//handle/11303/7520.3#

Grundstein, A., & Cooper, E. (2018). Assessment of the Australian Bureau of Meteorology wet bulb globe temperature model using weather station data. *International Journal of Biometeorology*, *62*(12), 2205–2213. https://doi.org/10.1007/s00484-018-1624-1

Gultepe, I. (2015). Mountain weather: Observation and modeling. *Advances in Geophysics*, *56*, 229–312. https://doi.org/10.1016/bs.agph.2015.01.001

Gultepe, I., Isaac, G. A., Joe, P., Kucera, P. A., Theriault, J. M., & Fisico, T. (2014). Roundhouse (RND) mountain top research site: Measurements and uncertainties for winter alpine weather conditions. *Pure and Applied Geophysics*, *171*(1–2), 59–85. https://doi.org/10.1007/s00024-012-0582-5

Heo, S., & Bell, M. L. (2019). Heat waves in South Korea: Differences of heat wave characteristics by thermal indices. *Journal of Exposure Science and Environmental Epidemiology*, *29*(6), 790–805. https://doi.org/10.1038/s41370-018-0076-3

Heo, S., Bell, M. L., & Lee, J. T. (2019). Comparison of health risks by heat wave definition: Applicability of wet-bulb globe temperature for heat wave criteria. *Environmental Research*, *168*, 158–170. https://doi.org/10.1016/J.ENVRES.2018.09.032

High Plains Regional Climate Center (HPRCC). (2020). Automated weather data network. Retrieved from https://hprcc.unl.edu/index.php

Hilliker, J. L., Akasapu, G., & Young, G. S. (2010). Assessing the short-term forecast capability of nonstandardized surface observations using the National Digital Forecast Database (NDFD). *Journal of Applied Meteorology and Climatology*, *49*(7), 1397–1411. https://doi.org/10.1175/2010JAMC2137.1

Hufkens, K., Basler, D., Milliman, T., Melaas, E. K., & Richardson, A. D. (2018). An integrated phenology modelling framework in r. *Methods in Ecology and Evolution*, *9*(5), 1276–1285. https://doi.org/10.1111/2041-210X.12970

Illinois State. (2019). Water and atmospheric resources monitoring Program - ICN: Stations map and information, Illinois state water survey [Dataset]. Retrieved from https://www.isws.illinois.edu/warm/icnsitemap.asp

Jared Rennie, J., Palecki, M. A., Heuser, S. P., & Diamond, H. J. (2021). Developing and validating heat exposure products using the U.S. climate reference network. *Journal of Applied Meteorology and Climatology*, *60*(4), 543–558. https://doi.org/10.1175/JAMC-D-20-0282.1

Justine, J., Monteiro, J. M., Shah, H., & Rao, N. (2023). The diurnal variation of wet bulb temperatures and exceedance of physiological thresholds relevant to human health in South Asia. *Communications Earth & Environment*, *4*(1), 1–11. https://doi.org/10.1038/s43247-023-00897-0

Kansas Mesonet. (2017). Kansas Mesonet historical weather [Dataset]. Retrieved from http://mesonet.k-state.edu/weather/historical/

Karger, D. N., Wilson, A. M., Mahony, C., Zimmermann, N. E., & Jetz, W. (2021). Global daily 1 km land surface precipitation based on cloud cover-informed downscaling. *Scientific Data*, *8*(1), 307. https://doi.org/10.1038/s41597-021-01084-6

Kilpelainen, T., Vihma, T., Lafsson, H., & Karlsson, P. E. (2011). Modelling of spatial variability and topographic effects over Arctic fjords in Svalbard. *Tellus A: Dynamic Meteorology and Oceanography*, *63*(2), 223–237. https://doi.org/10.1111/j.1600-0870.2010.00481.x

Klinges, D. H., Duffy, J. P., Kearney, M. R., & Maclean, I. M. D. (2022). MCERA5: Driving microclimate models with ERA5 global gridded climate data. *Methods in Ecology and Evolution*, *13*(7), 1402–1411. https://doi.org/10.1111/2041-210X.13877

Kong, Q., & Huber, M. (2022). Explicit calculations of wet-bulb globe temperature compared with approximations and why it matters for labor productivity. *Earth's Future*, *10*(3), e2021EF002334. https://doi.org/10.1029/2021EF002334

Lemke, B., Kjellstrom, T., Varghese, B., Hansen, A., Williams, S., Bi, P., & Pisaniello, D. (2019). Epidemiological descriptions of occupational health effects of climate change. *Occupational and Environmental Medicine*, *76*(Suppl 1), A72–A73. https://doi.org/10.1136/OEM-2019-EPI.193

Liljegren, J. C., Carhart, R. A., Lawday, P., Tschopp, S., & Sharp, R. (2008). Modeling the wet bulb globe temperature using standard meteorological measurements. *Journal of Occupational and Environmental Hygiene*, *5*(10), 645–655. https://doi.org/10.1080/15459620802310770

Liston, G. E. (2004). Representing subgrid snow cover heterogeneities in regional and global models. *Journal of Climate*, *17*(6), 1381–1397. https://doi.org/10.1175/1520-0442(2004)017<1381:RSSCHI>2.0.CO;2

Michigan State University. (2020). Michigan automated weather network [Dataset]. Retrieved from https://mawn.geo.msu.edu/

Mishra, A. K., & Ramgopal, M. (2015). An adaptive thermal comfort model for the tropical climatic regions of India (Köppen climate type A). *Building and Environment*, *85*, 134–143. https://doi.org/10.1016/j.buildenv.2014.12.006

Missouri Mesonet. (2020). Missouri Mesonet - AgEBB [Dataset]. Retrieved from http://agebb.missouri.edu/weather/stations/

Monson, R. K., & Baldocchi, D. D. (2014). Terrestrial biosphere-atmosphere fluxes. Retrieved from https://books.google.co.kr/books?hl=en&lr=&id=nXLgAgAAQBAJ&oi=fnd&pg=PR11&dq=+Monson,+R.,+%26+Baldocchi,+2014&ots=lgZ7t-MvgN&sig=zndD0A7uakTFeF_hrF4UAwRMIdw#v=onepage&q&f=false

Mott, R., Faure, F., Lehning, M., Löwe, H., Hynek, B., Michlmayer, G., et al. (2008). Simulation of seasonal snow-cover distribution for glacierized sites on Sonnblick, Austria, with the Alpine3D model. *Annals of Glaciology*, *49*, 155–160. https://doi.org/10.3189/172756408787814924

Napoly, A., Grassmann, T., Meier, F., & Fenner, D. (2018). Development and application of a statistically-based quality control for crowdsourced air temperature data. *Frontiers in Earth Science*, *6*(August), 1–16. https://doi.org/10.3389/feart.2018.00118

National Centers for Environmental Information. (2017). U.S. billion-dollar weather and climate disasters.

National Institute for Occupational Safety and Health (NIOSH). (2016). NIOSH criteria for a recommended standard: Occupational exposure to heat and hot environments. Retrieved from https://www.cdc.gov/niosh/docs/2016-106/pdfs/2016-106.pdf

National Weather Service Headquarters. (2022a). Service change notice 22-43 updated. Retrieved from https://www.weather.gov/media/notification/pdf2/scn22-43_wet_bulb_globe_temp_t2o_aaa.pdf

National Weather Service Headquarters. (2022b). Wet bulb globe temperature provision in the national digital forecast database (NDFD) product description document. Retrieved from https://www.weather.gov/mdl/ndfd_home

New Mexico State University. (2020). NM climate center | New Mexico State University - BE BOLD. Shape the future [Dataset]. Retrieved from https://weather.nmsu.edu/ziamet/request/station/nmcc-cr-1/data/

North Carolina State University. (2020). North Carolina state climate office – A public Service center [Dataset]. Retrieved from https://climate.ncsu.edu/

North Dakota Agriculture Weather Network Center. (2020). North Dakota agriculture weather network [Dataset]. Retrieved from https://ndawn.ndsu.nodak.edu/station-info.html?station=104

Oke, T. R. (1982). The energetic basis of the urban heat island. *Quarterly Journal of the Royal Meteorological Society*, *108*(455), 1–24. https://doi.org/10.1002/qj.49710845502

Oregon State University. (2022). PRISM climate group [Dataset]. Retrieved from https://prism.oregonstate.edu/

Page, W. G., Wagenbrenner, N. S., Butler, B. W., Forthofer, J. M., & Gibson, C. (2018). An evaluation of NDFD weather forecasts for wildland fire behavior prediction. *Weather and Forecasting*, *33*(1), 301–315. https://doi.org/10.1175/WAF-D-17-0121.1

Parks, R. M. (2022). ERA5 daily weather grids converted into national and sub-national boundaries worldwide [ComputationalNotebook]. Retrieved from https://github.com/rmp15/ERA5-grids-into-national-subnational-boundaries-Worldwide

Parks, R. M., Bennett, J. E., Tamura-Wicks, H., Kontis, V., Toumi, R., Danaei, G., & Ezzati, M. (2020). Anomalously warm temperatures are associated with increased injury deaths. In *Nature medicine* (Vol. 26, No. (1), pp. 65–70). Nature Research. https://doi.org/10.1038/s41591-019-0721-y

Parks, R. M., Rowland, S. T., Do, V., Boehme, A. K., Dominici, F., Hart, C. L., & Kioumourtzoglou, M.-A. (2023). The association between temperature and alcohol- and substance-related disorder hospital visits in New York State. *Communication and Medicine*, *3*(1), 1–9. https://doi.org/10.1038/s43856-023-00346-1

Patel, T., Mullen, S. P., & Santee, W. R. (2013). Comparison of methods for estimating wet-bulb globe temperature index from standard meteorological measurements. *Military Medicine*, *178*(8), 926–933. https://doi.org/10.7205/MILMED-D-13-00117

Perry, M., & Hollis, D. (2005). The generation of monthly gridded datasets for a range of climatic variables over the UK. *International Journal of Climatology*, *25*(8), 1041–1054. https://doi.org/10.1002/joc.1161

Reeve, M. A., & Kolstad, E. W. (2011). The spitsbergen South Cape tip jet. *Quarterly Journal of the Royal Meteorological Society*, *137*(660), 1739–1748. https://doi.org/10.1002/qj.876

Rennie, J. J., Palecki, M. A., Heuser, S. P., & Diamond, H. J. (2021). Developing and validating heat exposure products using the U.S. Climate reference network. *Journal of Applied Meteorology and Climatology*, *60*(4), 543–558. https://doi.org/10.1175/jamc-d-20-0282.1

Rothfusz, L. P. (1990). The heat index "equation" (or, more than you ever wanted to know about heat index).

Rupp, D. E., Daly, C., Doggett, M. K., Smith, J. I., & Steinberg, B. (2022). *Mapping an observation-based global solar irradiance climatology across the Conterminous United States*. American Meteorological Society. https://doi.org/10.1175/JAMC-D

Rusticucci, M., & Vargas, W. (1995). Seasonal and diurnal patterns of dry- and wet-bulb temperatures over Argentina. *International Journal of Climatology*, *15*(11), 1273–1282. https://doi.org/10.1002/JOC.3370151107

Slater, A. G. (2016). Surface solar radiation in North America: A comparison of observations, reanalyses, satellite, and derived products. *American Meteorological Society*, *17*(1), 401–420. https://doi.org/10.1175/JHM-D-15

Sonntag, D. (1990). Important new values of the physical constants of 1986, vapour pressure formulations based on the ITS-90, and psychrometer formulae. *Zeitschrift für Meteorologie*, *40*(5), 340–344.

Sousa, P. M., Trigo, R. M., Russo, A., Geirinhas, J. L., Rodrigues, A., Silva, S., & Torres, A. (2022). Heat-related mortality amplified during the COVID-19 pandemic. *International Journal of Biometeorology*, *66*(3), 1–12. https://doi.org/10.1007/s00484-021-02192-z

South Alabama. (2020). South Alabama Mesonet [Dataset]. Retrieved from http://chiliweb.southalabama.edu/archived_data.php

Spangler, K. R., Liang, S., & Wellenius, G. A. (2022). Wet-bulb globe temperature, universal thermal climate index, and other heat metrics for US counties, 2000–2020. *Scientific Data*, *9*(1), 326. https://doi.org/10.1038/s41597-022-01405-3

Spangler, K. R., Weinberger, K. R., & Wellenius, G. A. (2019). Suitability of gridded climate datasets for use in environmental epidemiology. *Journal of Exposure Science and Environmental Epidemiology*, *29*(6), 777–789. https://doi.org/10.1038/s41370-018-0105-2

Spangler, K. R., & Wellenius, G. A. (2021). Spatial and intraseasonal variation in changing susceptibility to extreme heat in the United States. *Environmental Epidemiology*, *5*(2), e136. https://doi.org/10.1097/EE9.0000000000000136

Steadman, R. G. (1979). A temperature-humidity index based on human physiology and clothing science. *Journal of Applied Meteorology*, *18*(7), 861–873. https://doi.org/10.1175/1520-0450(1979)018<0861:taospi>2.0.co;2

STEM. (2020). Weather STEM [Dataset]. Retrieved from https://franklin-oh.weatherstem.com/data

Stull, R. (2011). Wet-bulb temperature from relative humidity and air temperature. *Journal of Applied Meteorology and Climatology*, *50*(11), 2267–2269. https://doi.org/10.1175/JAMC-D-11-0143.1

The National Oceanic and Atmospheric Administration. (2023). Heat forecast tools. Retrieved from https://www.weather.gov/safety/heat-index

Thornton, P. E., Running, S. W., & White, M. A. (1997). Generating surfaces of daily meteorological variables over large regions of complex terrain. *Journal of Hydrology*, *190*(3–4), 214–251. https://doi.org/10.1016/S0022-1694(96)03128-9

Thornton, P. E., Shrestha, R., Thornton, M., Kao, S. C., Wei, Y., & Wilson, B. E. (2021). Gridded daily weather data for North America with comprehensive uncertainty quantification. *Scientific Data*, *8*(1), 1–17. https://doi.org/10.1038/s41597-021-00973-0

Thornton, P. E., Shrestha, R., Thornton, M. M., Kao, S. C., Wei, Y., & Wilson, B. E. (2020). Gridded daily weather data for North America with comprehensive uncertainty quantification (pp. 1–25).

Tripp, B., Vincent, H. K., Bruner, M., & Smith, M. S. (2020). Comparison of wet bulb globe temperature measured on-site vs estimated and the impact on activity modification in high school football. *International Journal of Biometeorology*, *64*(4), 593–600. https://doi.org/10.1007/s00484-019-01847-2

Tscholl, S., Tasser, E., Tappeiner, U., & Egarter Vigl, L. (2022). Coupling solar radiation and cloud cover data for enhanced temperature predictions over topographically complex mountain terrain. *International Journal of Climatology*, *42*(9), 4684–4699. https://doi.org/10.1002/joc.7497

Tuholske, C. (2021). GlobalUrbanHeat [ComputationalNotebook]. Retrieved from https://github.com/ecohydro/GlobalUrbanHeat/blob/main/src/05_HI-to-WBGT.py

Tuholske, C., Caylor, K., Funk, C., Verdin, A., Sweeney, S., Grace, K., et al. (2021). Global urban population exposure to extreme heat. *Proceedings of the National Academy of Sciences of the United States of America*, *118*(41), 1–9. https://doi.org/10.1073/pnas.2024792118

Uejio, C. K., Morano, L. H., Jung, J., Kintziger, K., Jagger, M., Chalmers, J., & Holmes, T. (2018). Occupational heat exposure among municipal workers. *International Archives of Occupational and Environmental Health*, *91*(6), 705–715. https://doi.org/10.1007/s00420-018-1318-3

Underwood, B. S., Guido, Z., Gudipudi, P., & Feinberg, Y. (2017). Increased costs to US pavement infrastructure from future temperature rise. *Nature Climate Change*, *7*(10), 704–707. https://doi.org/10.1038/nclimate3390

United States Department of Agriculture. (2020). Natural resources conservation service [Dataset]. Retrieved from https://www.nrcs.usda.gov/wps/portal/nrcs/site/national/home/

United States Environmental Protection Agency. (2020). Climate change indicators: Heat-related deaths | US EPA. Retrieved from https://www.epa.gov/climate-indicators/climate-change-indicators-heat-related-deaths

University of Arizona. (2020). The Arizona meteorological network [Dataset]. Retrieved from https://cals.arizona.edu/AZMET/az-data.htm

University of Florida. (2020). FAWN - Florida automated weather network [Dataset]. Retrieved from https://fawn.ifas.ufl.edu/

U.S Global Change Research Program. (2023). Fifth national climate assessment. Retrieved from https://www.globalchange.gov/nca5

Washington State University. (2020). Hourly data | AgWeatherNet at Washington state University [Dataset]. Retrieved from http://weather.wsu.edu/?p=92950

Weatherly, J. W., & Rosenbaum, M. A. (2017). Future projections of heat and fire-risk indices for the contiguous United States. *Journal of Applied Meteorology and Climatology*, *56*(4), 863–876. https://doi.org/10.1175/JAMC-D-16-0068.1

Yaglou, C. P., & Minaed, D. (1957). Control of heat casualties at military training Centers. *Arch. Indust. Health*, *16*(4), 302–316. Retrieved from https://www.cabdirect.org/cabdirect/abstract/19582900896

Yang, D., & Bright, J. M. (2020). Worldwide validation of 8 satellite-derived and reanalysis solar radiation products: A preliminary evaluation and overall metrics for hourly data over 27 years. *Solar Energy*, *210*, 3–19. https://doi.org/10.1016/j.solener.2020.04.016

Zardi, D., & Whiteman, C. D. (2013). *Diurnal mountain wind systems* (pp. 35–119). Springer Atmospheric Sciences. Mountain Weather Research and Forecasting. Retrieved from https://www.pmf.unizg.hr/_download/repository/Zardi-Whiteman_Chptr2%5B1%5D.pdf

Zhang, Y., & Shindell, D. T. (2021). Costs from labor losses due to extreme heat in the USA attributable to climate change. *Climatic Change*, *164*(3–4), 1–18. https://doi.org/10.1007/s10584-021-03014-2